CNRS
Centre National de la Recherche Scientifique

INFN
Istituto Nazionale di Fisica Nucleare

Transient power drop in dark fringe lock acquisition during the commissioning before O3

A. Allocca[1,*], A. Chiummo[2], P. Ruggi[2], and H. Yamamoto[3]

[1] *INFN - Sezione di Pisa*
[2] *EGO - European Gravitational Observatory*
[3] *LIGO Laboratory, California Institute of Technology*

VIR-1047A-19

[*] *corresponding author:* allocca@pi.infn.it

VIRGO* A joint CNRS-INFN Project - EGO* the site of the VIRGO project
Via E. Amaldi, I-56021 S. Stefano a Macerata - Cascina (Pisa)
Secretariat: Telephone (39) 050 752 521 * FAX (39) 050 752 550 * Email: ego@ego-gw.it

Contents

1 Introduction

The Advanced Virgo interferometer is designed to be operated at *dark fringe*: this means that, ideally, a completely destructive interference has to be achieved at the anti-symmetric port [4]. When this configuration is reached, by means of suitable servo-control loops on the mirror positions and alignments, the laser power stored in the arm Fabry-Perot is of the order of ~ 6000 times the input power coupled to the ITF mode. This power depends on the recycling gain of the *Power Recycling Cavity* (PRC) which, in turn, depends on the effective average reflectivities of the arms and so on the *Round-Trip Losses* (RTL) of the arm cavities.
Back in Spring 2017, we achieved for the first time the dark fringe working point and a sufficient lock robustness to witness a legitimate steady state. The dark fringe lock is acquired by means of what is called the *variable finesse technique*, in which the power recycling mirror is aligned when the Michelson working point is kept at half fringe, and therefore this latter gets progressively reduced, until reaching the destructive interference condition at dark fringe. During this process, the recycling cavity gain (and therefore the circulating power) increases until reaching a value of about 38. Since the very first achievements, each time the dark fringe lock is acquired, power stored in the arms experiences a transient drop from a given initial value down to some $\sim 10\%$ less in the steady state with a time constant of the order of minutes. Furthermore, when the input power was increased from the initial $Pin \sim 14W$ to the later set $Pin \sim 25W$, the power drop became even worse and we lose some $\sim 30\%$ of the initial value of the power stored in the arms (see figure 6).
This phenomenon has many implications. The transient power drop after acquiring dark fringe lock is unfortunate already *per se*, because it makes the input power increase less effective, by as much as 70% in the worst experienced case. Furthermore, this phenomenon could be a symptom for something even worse occurring at the mirrors, such as surface contamination, therefore the understanding of this unknown process is mandatory, in order to exclude potential threat such as mirror degradation etc... .
One more potentially bad implication of this power loss is the impact on squeezed vacuum effect. Since this power loss could be related to a decreased effective reflectivity as seen from the anti-symmetric port, this could turn into increased losses experienced by the injected squeezed vacuum, so making it less effective in reducing the shot noise impact on sensitivity.
For all of these reasons, the understanding and mitigation of this phenomenon has a very high priority, mostly in view of the upgrades foreseen for the next Advanced Virgo plus phases.
This note is intended as a compound of the understanding of the phenomenon up to the end of 2018, summarizing what was presented in [1] and [2], besides many logbook entries on the topic.

2 Power drop description

Since the very beginning of the AdV operation in dark fringe, a peculiar behavior can be noticed in the power evolution during the lock acquisition. Just after the dark fringe transition, the power as seen by the photodiodes in transmission from the arms (B7, B8) and by the photodiodes monitoring the power in the recycling cavity (B4, B5) begins to drop (figure 4).
A loss of power could suggest a possible misalignment immediately after the dark fringe transition, but it has been experimentally verified not to be the case [3]. This points towards a different kind of process at the origin of this effect.
In order to get a hint about the possible cause, few simple Finesse simulations have been performed to look at the power at different ports and compare their trend with the real data. These simulations accounted for several cases: a) input beam not well matched to the cavity mode (figure 1); b) intracavity losses increase in one of the arm cavities (figure 2); c) intracavity losses increase in both the arm cavities (figure 3).

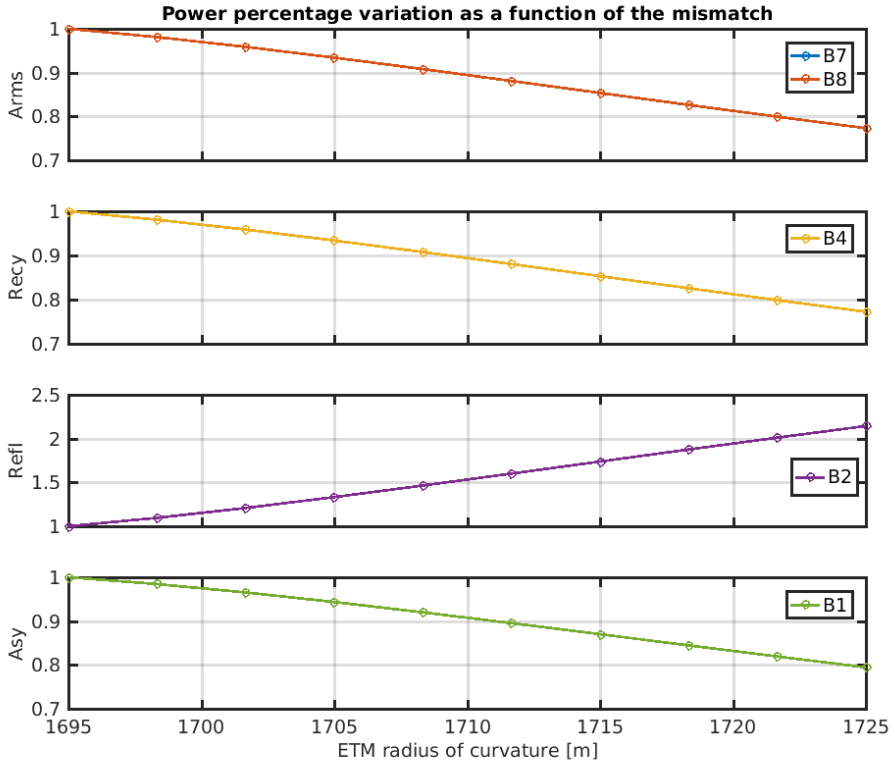

Figure 1: Finesse simulation of power at different ports as a function of the End Test Masses radii of curvature while keeping the input beam parameters fixed. From the top plot: arms transmission (B7, B8), recycling cavity power (B4), power at the reflection port (B2) and power at the antisymmetric port (B1). Aberrations and high order modes not included. The power drops at every ITF port, besides the reflection which instead increases.

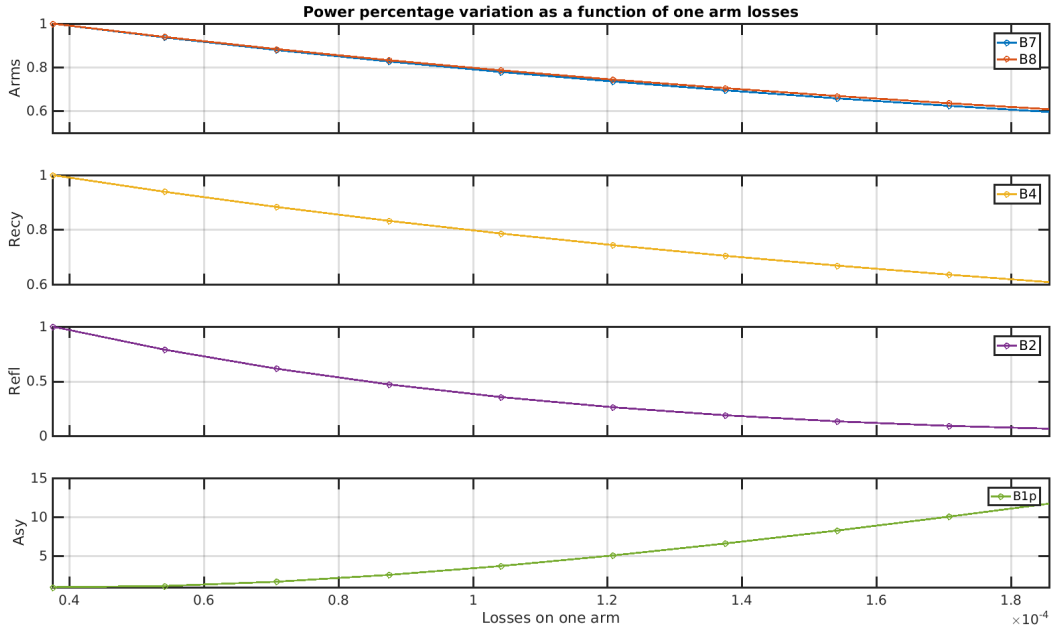

Figure 2: Finesse simulation of power at different ports while varying the losses in one of the arms. Aberrations and high order modes not included. Also in this case the power in the arms and in the recycling cavity decreases but, unlike the mismatch case, the power drops also at the reflection port, while increases at the dark port.

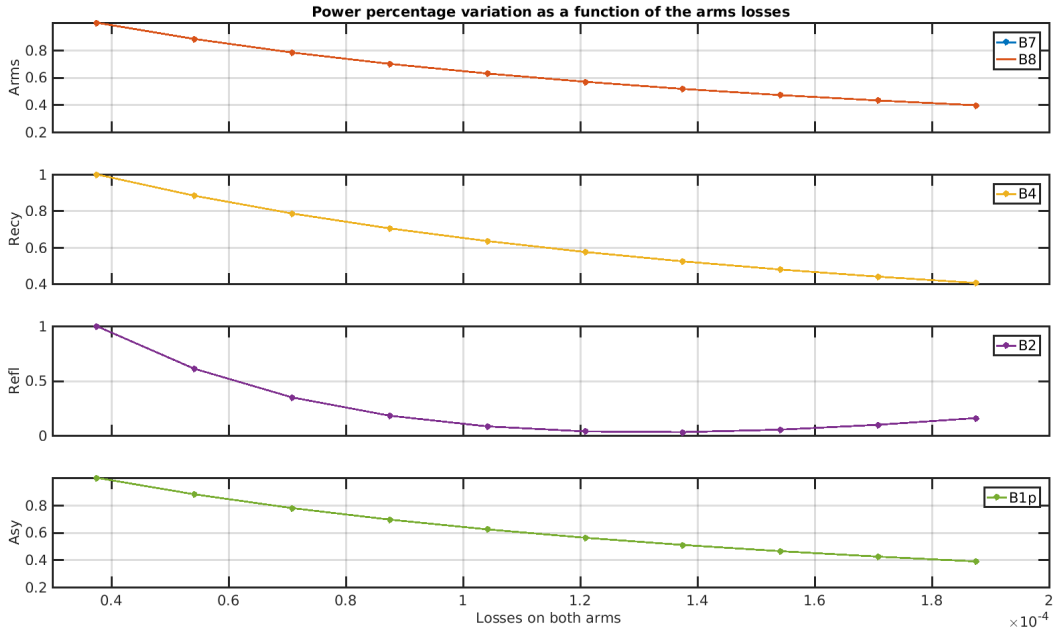

Figure 3: Finesse simulation of power at different ports while varying the losses in both the arms. Aberrations and high order modes not included. This is the only case where the power decreases at all the ports.

A mismatch could be induced, for instance, by the substrates heating due to the high circulating power or to an increase of losses in the interferometer. In this case, the drop of the circulating power and at the dark port corresponds to an increase of power back reflected off the power recycling mirror PR (monitored by the B2 photodiode).
In the case of losses, we must distinguish whether the process happens in one of the arms or both of them, pointing to a big or small losses asymmetry between the arms. In the first case, power is observed to decrease in both the arms, in the recycling cavity and at the reflection port. More precisely, on B2 the power decreases until the critical coupling is reached, after which it starts increasing again. Furthermore, unlike the matching case, the power at the dark port increases. In the second case, instead, when the losses are present in both the arms, the dark fringe experiences a different behavior, as the power decreases also at this port. Any intermediate case (i.e.: non equal losses in the arms), brings the power at the antisymmetric port to decrease first and then increase again, after a certain threshold value.

In figure 4 the signals of the interferometer are shown. Considering that the back-reflection decreases with similar trend as for arms transmitted power (top plot in figure 4), the mismatch hypothesis is discarded, rather pointing towards an increase of losses in the ITF. To distinguish between the one arm / two arms losses cases, we look at the trend of B1p photodiode. For a complete picture, we should consider that B1p is contaminated by the DC component of the sideband fields (witnessed by the B4_112MHz channel), which slightly increase after the dark fringe transition as shown in fig. 5. Therefore, since the power on B1p stays almost constant, this seems to suggest that a losses increase process is happening in both the arms. Finally, since the sidebands only resonate in the central interferometer (CITF), this seems to suggest that the power drop process is linked to something occurring outside the recycling cavity,pointing again to the arms as main responsible for this process.

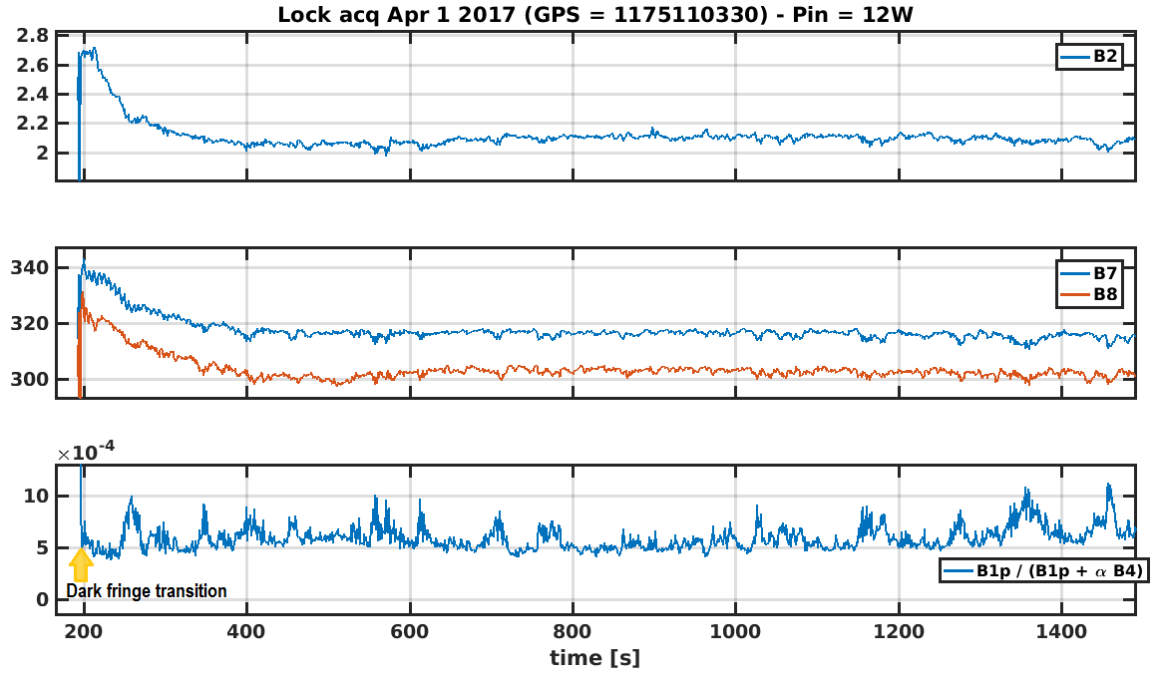

Figure 4: Power drop phenomenon happening right after the dark fringe transition. The arms transmitted power and the dark fringe transmissivity are shown in the second and third subplots, respectively. The dark fringe transition is indicated by the yellow arrow in the third subplot. The first subplot shows the power reflected by the interferometer, which has a similar trend.

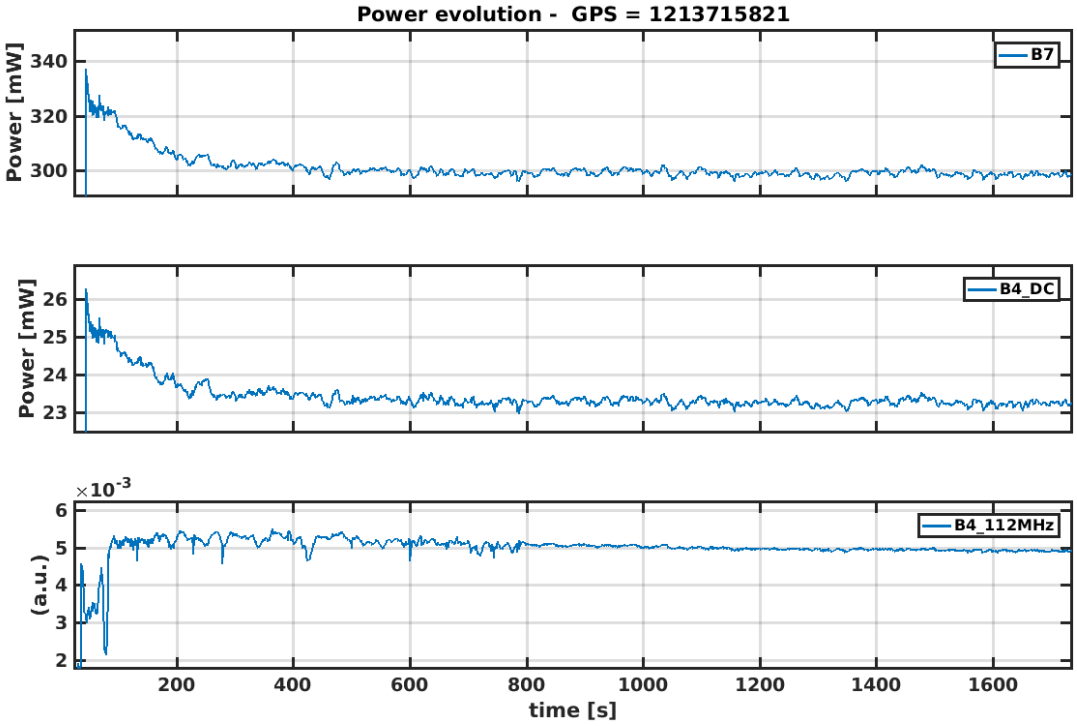

Figure 5: Interferometer signals during the transient right after dark fringe acquisition. In particular, top is the North arm transmission, middle is the pick-off reflection at the level of the PR mirror inside the power recycling cavity, DC power, while bottom is the same pick-off but demodulated at 2f of the RF used for the lock, namely the sideband power. While both the transmission from the North arm and the carrier power inside the PRM experience similar evolution, the sideband power evolution is rather different, so hinting to some process occurring only in the arm as a responsible for the power drop.

2.1 Power drop percentage and time constant

The power drop phenomenon has been analyzed in several interferometer configurations characterized by different injected power. All the configurations and relative time periods are summarized in table 1.

Period	Input Power
Aug 2017 (O2)	14W
Nov 2017	26W
Apr 2018 (After monolithic installation)	12W
Jul 2018 (Increased power)	25W
Nov 2018	18W

Table 1: List of different input power configurations.

As shown in figure 6 the power drop percentage changes with the input power: the higher the injected power, the deeper the drop.
Another feature of this phenomenon is that also the time constant of the drop process doesn't seem to show an evident dependence on the injected power (from around 101s with Pin = 15W to 80s with Pin = 25W) as reported in figure 7. If a dependence exists, it seems to be rather small.

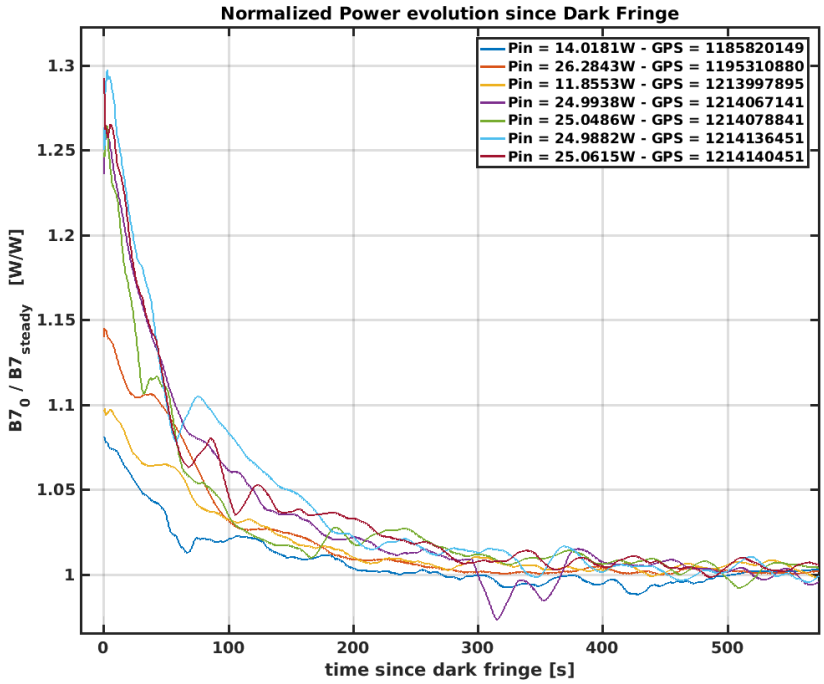

Figure 6: Power drop normalized to the steady state for different input power configurations. The higher the input power, the higher the drop percentage. Notice that the second trace (red) corresponds to the first time we went to high power. After that, a break for the installation of the monolithic suspensions took place. When operations started again, the drop percentage had worsened with respect to the past.

3 A few hypotheses

Among the hypotheses which were considered to explain this phenomenon, some were proved to be not consistent with the observations and therefore discarded. In particular:

- Non-optimal coupling:
  The early observation of the transient power drop led to several hypotheses to explain the loss of circulating power. Most of those hypotheses, as reported in Section 2 were based on a non-optimal coupling of power into the ITF mode, evolving with time after the dark fringe acquisition: among them we took into account injected field mode mismatch, misalignment, unwanted longitudinal offsets in the control loops. As shown in figure1, the distinctive features of all these hypotheses is that the increase of uncoupled power makes the reflected power increase as well. Instead, during the typical transient after the dark fringe acquisition, a *decrease* of the reflected power is observed on the B2 photodiode (see figure 4). This behavior is only explained by increasing losses in the ITF (see figures 2, 3).

- Sensor response:
  One other briefly considered hypothesis was a possible sensor heating changing the response of the photodiodes with time, or in other words a *fake drop*. That was tested by looking at different kind of sensors, such as quadrant photodiodes (with much larger surface) and IR cameras (with very faint impinging power). All of these sensors showed the same transient for the arm stored power, so confirming that the power drop is a real issue. Figures 8 and 9.

- Increase of losses
  In order to check if this phenomenon is related to an increase of transmissivity towards the dark port, we measured the carrier recycling gain in the power recycling cavity, as seen in transmission from the

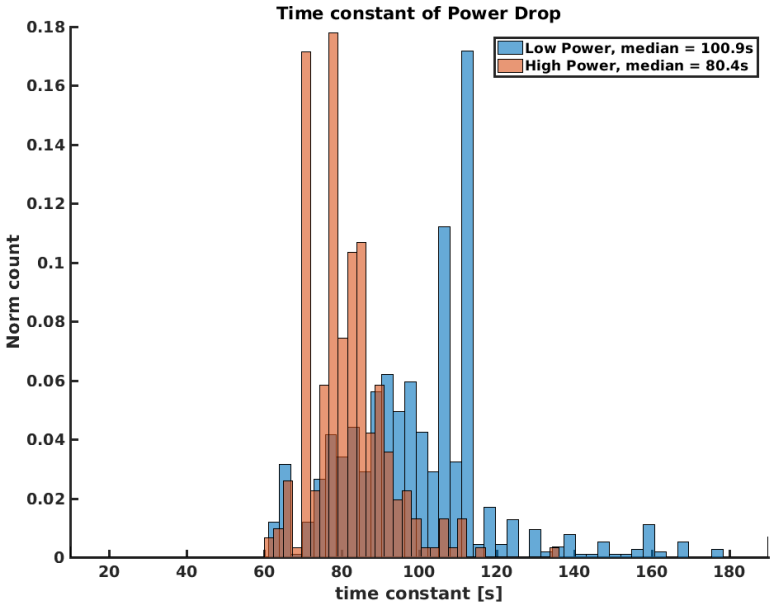

Figure 7: Time constant distribution of the power drop transient for low input power (<18W) and high input power (>18W). The time constant distributions seem to overlap for a large extent, and if a dependence on the input power exists, it is very small.

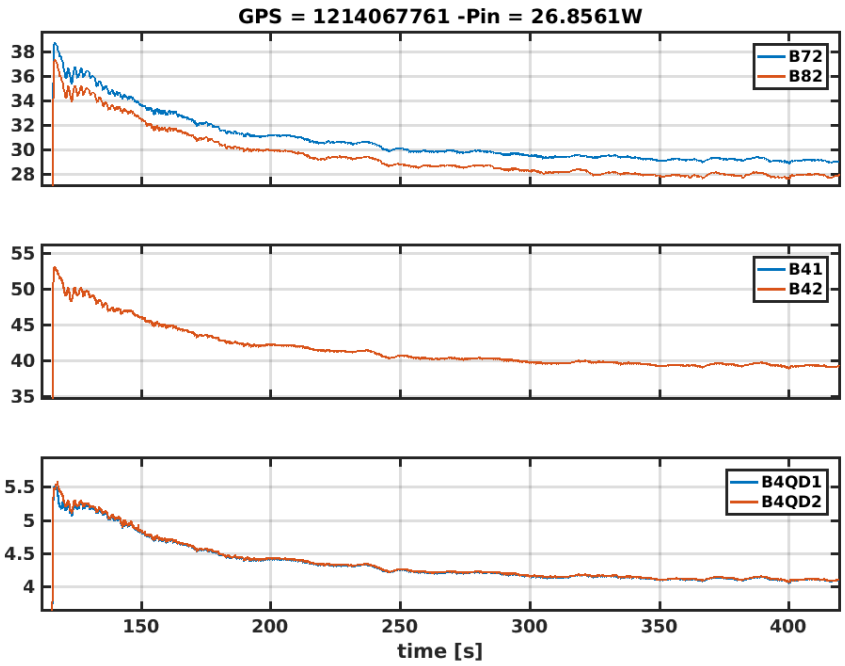

Figure 8: Power recorded by two different kinds of sensors: photodiodes B7/8/4, and quadrants B4QD. The behavior is very similar, which points towards something really happening in the interferometer.

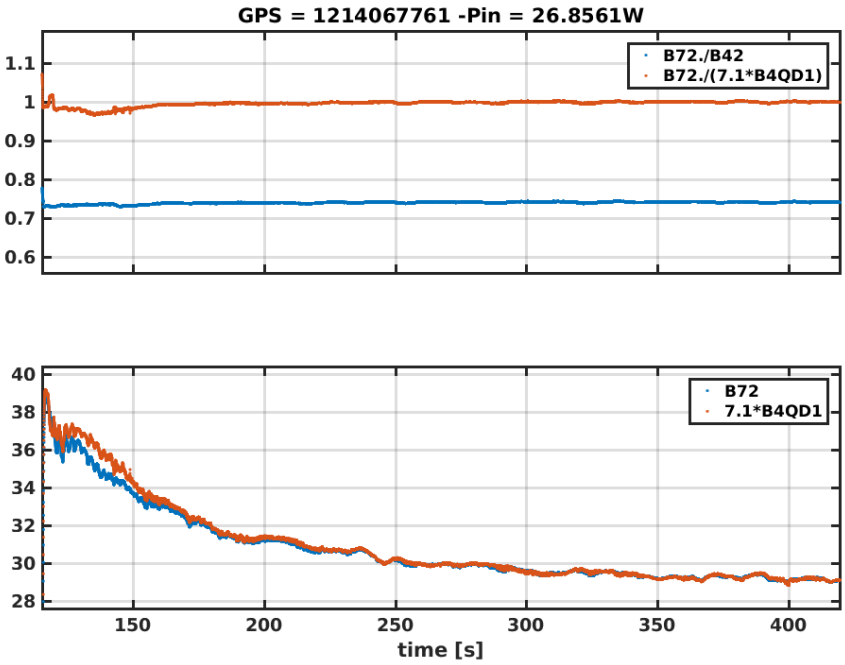

Figure 9: Upper plot: ratio between two different kinds of sensors (photodiodes and quadrant photodiodes), which stays constant. Bottom plot: comparison between B7 and B4 QPD trends: they behave the same.

arm cavities. This makes a clear measurement of the carrier recycling gain inside the PRC, since the sidebands are anti-resonant in the locked arms and so totally reflected. From that measurement we derive the equivalent arm RTL needed to match the gain.
The expected PRC recycling gain for the carrier reads as:

$$G_{prc} = \left| \frac{t_{PR}}{1 - r_{ARM}\ r_{PR}\ \sqrt{1 - (G_{arm}\ RTL_{arm} + T_{ASY})}} \right|^2 \tag{3.1}$$

where $G_{arm} = 287$ is the arm gain, r_{ARM} is the common arm field reflectivity without losses (*i.e.* $r_{ARM} = 1$ for AdV) and r_{PR} is the power recycling mirror field reflectivity. The carrier recycling gain in the PRC is denoted G_{prc}, and T_{ASY} is the fringe condition, defined as:

$$T_{ASY} = \frac{B1p}{B1p + \alpha B4} \qquad (\alpha = 10.47) \tag{3.2}$$

where α is the factor needed to equalize the B1p and B4 photodiodes at half fringe in recombined configuration.
The equivalent arm RTL needed to match the observed recycling gain are computed by solving the previous equation:

$$RTL_{arm} = \frac{1}{G_{arm}} \left[(1 - T_{ASY}) - \frac{1}{(r_{ARM}^2\ r_{PR}^2)} \left(1 - \frac{t_{PR}}{\sqrt{(G_{prc})}} \right)^2 \right] \tag{3.3}$$

Figures 10 show the evolution of the carrier recycling gain after the dark fringe transition (left y-axis). On the same figures, the equivalent average losses in the arms needed to match the observed gain is plotted,

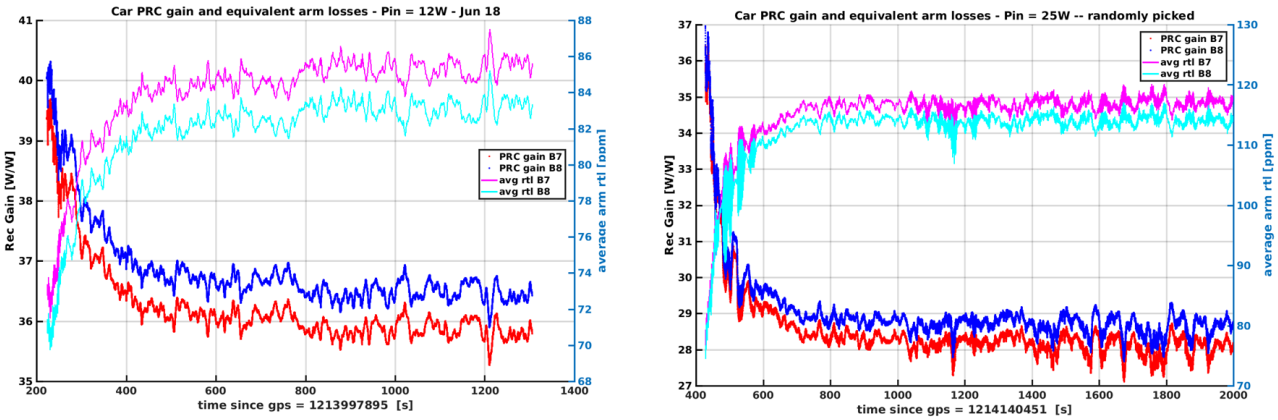

Figure 10: Power drop (left y-axis) and equivalent round trip losses (right y-axis) for two different input power configurations.

as if no losses other than the dark port transmission were in the CITF (right y-axis). The fact that we need to add increasing equivalent arm losses to match the recycling gain means that this drop of power cannot be completely explained by the evolution of the dark port transmission.

A fit of the time constant of the losses has been also performed, and the result is shown in figure 11.

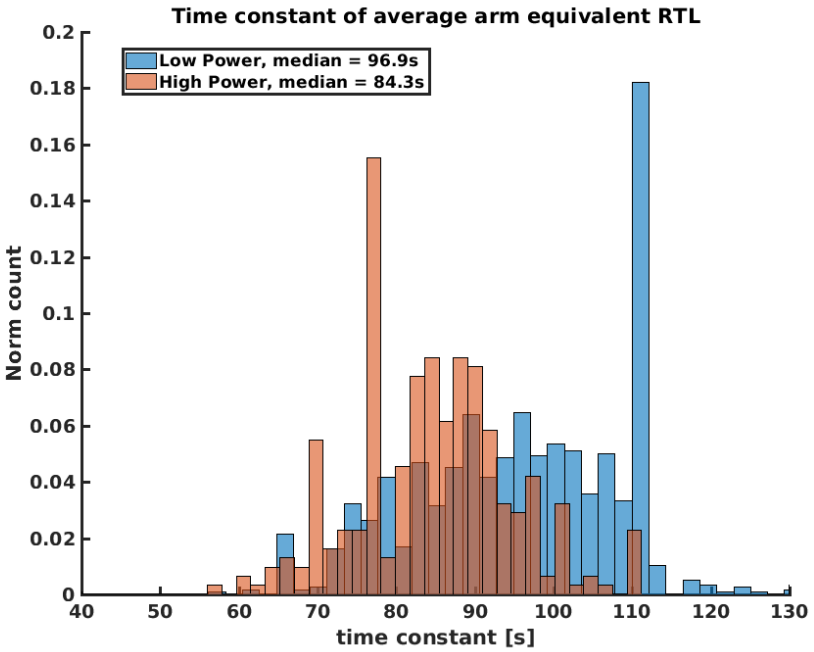

Figure 11: Time constant distribution of the equivalent RTL for low input power (<18W) and high input power (>18W). Only a slight change of time constant as a function of the input power is recognizable in this distribution.

Also in this case, only a slight change of time constant as a function of the input power is recognizable in this distribution.

A tentative conclusion from this analysis is that there are additional RTL onsetting in the arms as a consequence of some slow process triggered by high circulating power in the arm, whose time constant does not vary significantly over different input powers, but whose amplitude does depend on the circulating power in the arm. Could this be compatible with the heating up of one or more small, anomalously absorbing points on the ETMS?

4 ITF circulating power recovery: experiments

4.1 Changing beam impact point on ETMs

The effect of a static misalignment of the arm cavity axes with respect to the beam direction has been excluded as the cause of the power drop happening during the dark fringe transition, since also the back-reflected power off the PR mirror shows a similar trend as the circulating power, and the power loss cannot be recovered by changing the mutual alignment of the mirrors with respect to the beam.
A different possibility was explored through another test, performed to check what happens if the beam is not sent towards the center of the terminal mirrors (as we properly use to do) , but towards a peripheral region of them, having care of keeping all the ITF optics aligned with respect to the new beam direction and the ITMs centered. Ideally, this experiment should not affect the power circulating in the arms, provide that the terminal mirrors have constant optical parameters over a large surface. However, going in a specific direction on both the end mirror surfaces it was possible to increase the recycled power, and at the same time improve the contrast at the dark port. Almost all the lost power was recovered when the beam was off-centered on both mirrors by about 2 cm (the off-centering was quite evident also looking by eye at the cameras pointing to NE and WE HR faces).
In figure 12, the arms transmitted power and the contrast are shown in top and bottom plot, respectively. The yellow arrow shows the start of the beam displacement on one of the ETMs, whose effect is to recover almost the same circulating power as the beginning of the dark fringe lock. At the same time, this action lowers the contrast defect, as shown in the bottom plot, and a picture of the dark port power distribution corresponding to the black stars points as seen by the phase camera is shown in figure 13.
The experiment has been repeated on both the arms, and in both cases a power increase corresponding to some preferred positions was found (fig. 14).
Even if this experiment identifies a configuration which allows to recover the effect of the power drop, unfortunately (and as expected) this beam miscentered position cannot be defined as a new working point, mainly because of the huge coupling of angular noise on the sensitivity.

4.2 Changing ETM RoCs

A possible explanation for the power drop is the scattering into high order modes which are close to the resonance of the fundamental mode and are, therefore, in turn put into resonance. This scattering process drags power away from the fundamental mode, increasing the losses for the carrier field. This hypothesis is supported by the dark fringe power distribution, where it is possible to recognize a TEM of order 8. Studies carried on the effect of mirror aberrations on Advanced Virgo interferometer [5] identified the conditions which can bring the 8th order mode close to the resonance. Such conditions are fulfilled in the current optical configuration [6], as the radii of curvature are slightly off with respect to the design.
If this is the process giving rise to the cavity power drop, it can be mitigated by moving the high order mode away from the resonance. This condition can be achieved by changing the radius of curvature of at least one of the Fabry-Perot cavity mirrors. This was the motivation which led to the use of the Ring Heater actuators on the ETMs [7]: indeed, changing the mirrors radii of curvature corresponds to the variation of the cavity Gouy phase, so the HOMs resonance conditions is no longer the same.
The RHs were operated at different powers in order to find a good working point to minimize the contrast, as it is shown in figure 15. Second and third plots from the left in fig.16 show the Dark port power distribution in the two different Ring Heater power, marked in figure 15 with black crosses. Changing the radii of curvature, the Dark port HOM content is clearly different with respect to the reference, which is the first from the left in fig. 16. More about the mode decomposition of the DF can be found in [8].

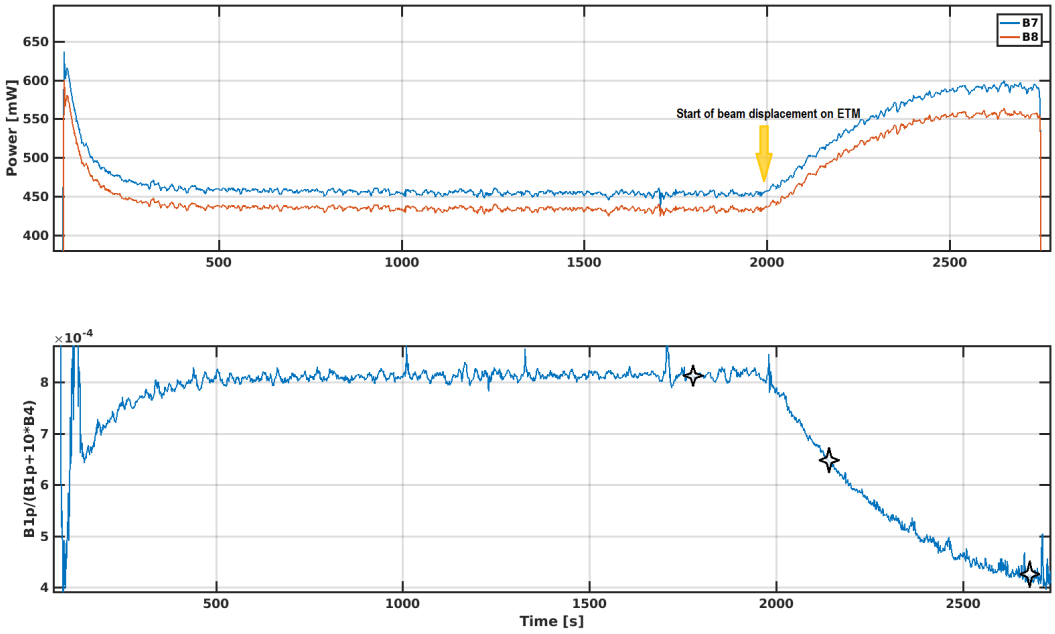

Figure 12: Top: power transmitted by North (B7) and West (B8) arms. Bottom: contrast. Displacing the beam on the ETM induces an increase of the circulating power and, at the same time, an improvement of the contrast. Corresponding to the black stars, the dark port power distribution is shown in figure 13.

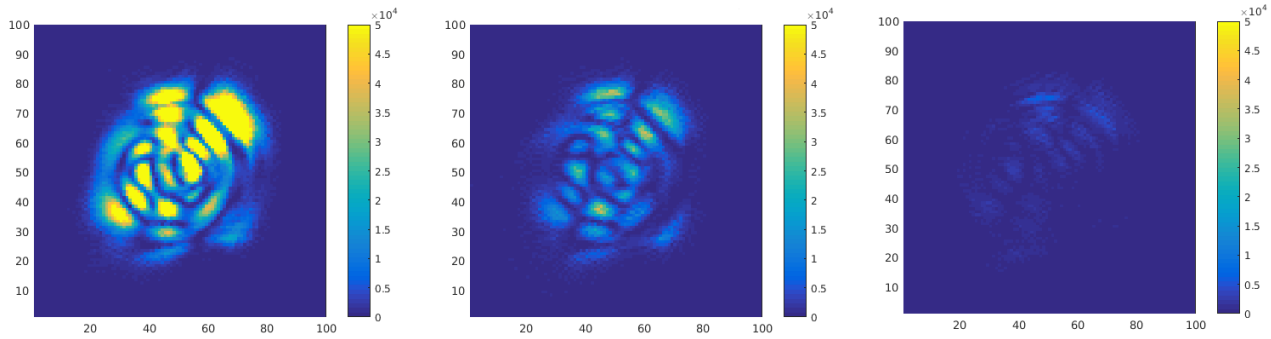

Figure 13: Dark fringe evolution during the miscentering experiment. The first image to the left shows the starting point. The signature of two high order modes are recognizable in the power distribution. Displacing the beam on the ETM does not affect the dark fringe mode content but rather decreases the power scattered in the high order modes, which makes the dark port beam darker and darker. The three images are taken in correspondence of the black stars in figure 12.

In this new working point, we recompute the effective arm RTL and estimate the variations in the three different configurations, which are *low power* (<18W), high power (>18W) and high power - RH on. An analysis has been carried on over about one year of data, and the results are shown in figure 17.

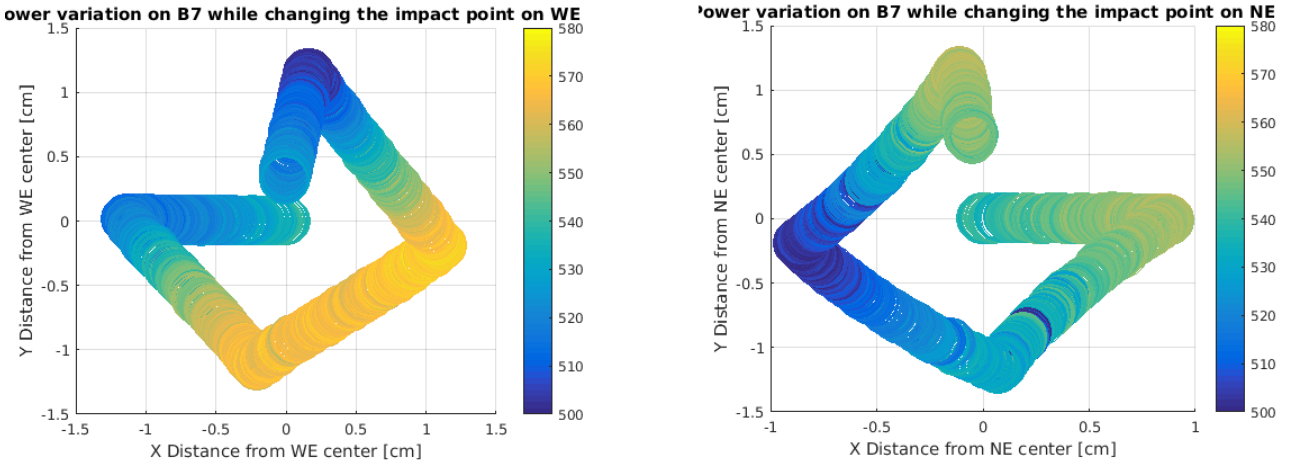

Figure 14: Arm transmitted power as a function of the beam position on the WE (left) and NE (right) mirror. The axes correspond to the distance from the mirror center, while the colors account for the circulating power in the arms. The beam displacement on the WE mirror seems to be more effective than the displacement on the NE.

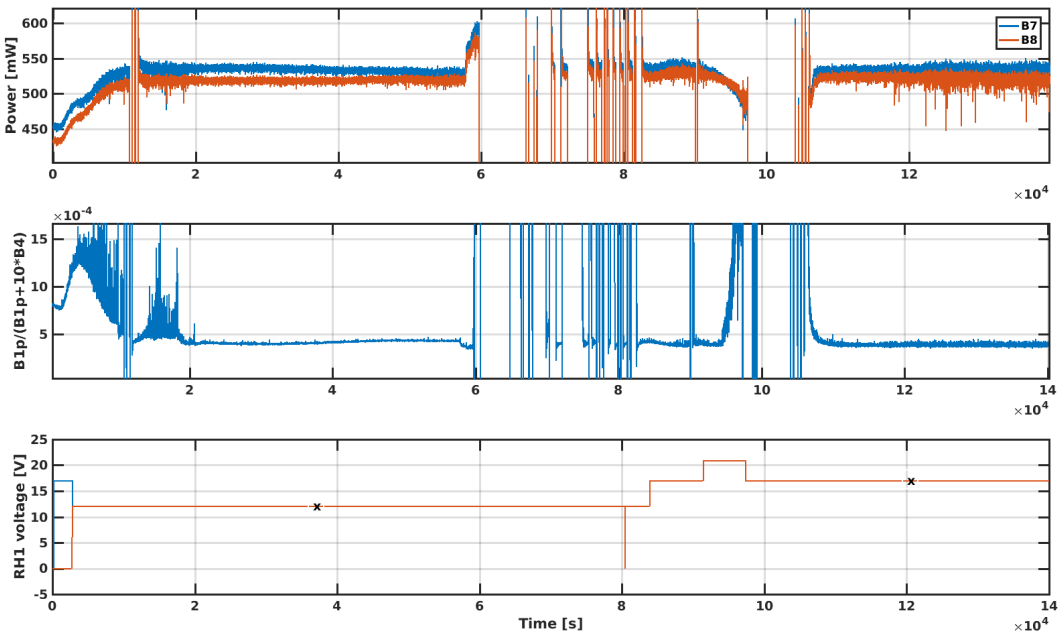

Figure 15: Top: Transmitted power from the North (B7) and West (B8) cavities. Center: Contrast. Bottom: Ring Heater voltage.

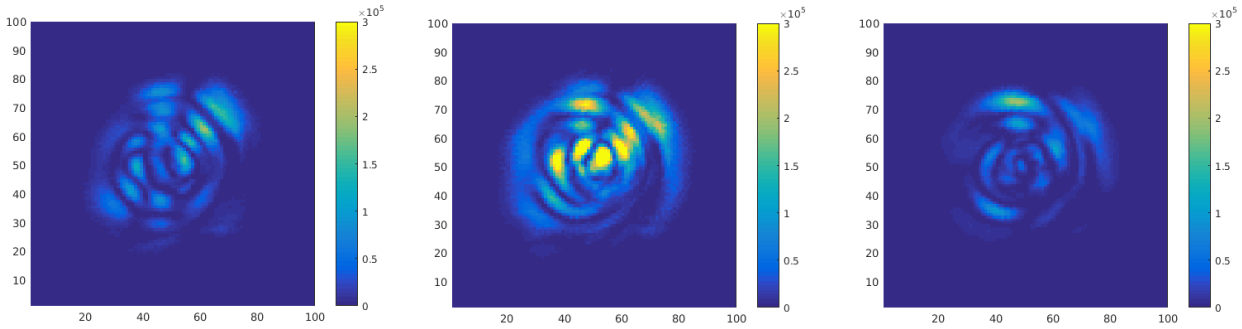

Figure 16: Power distribution at the dark port as seen by the Phase Camera. The first figure from the left corresponds to the configuration with no RH, while the second and the third correspond to the configurations marked with a black cross in figure 15.

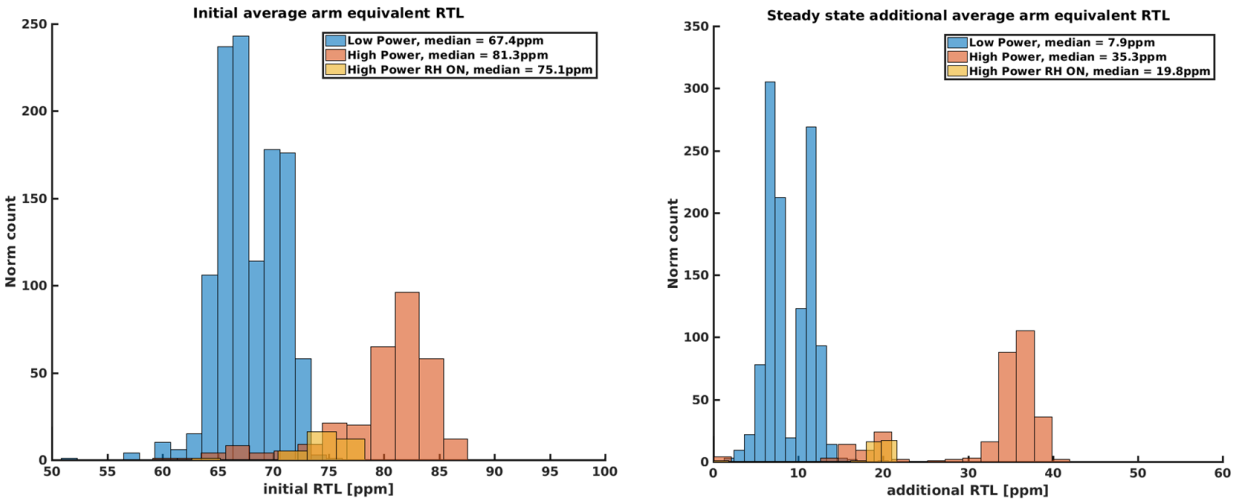

Figure 17: Left: Equivalent arm RTL to be added in order to match the measured carrier recycling gain at the beginning of the dark fringe lock. Right: Additional equivalent arm RTL needed to match the carrier recycling gain at the steady state. The measurements are taken over about one year of data, and in three different configuration. See text for more details.

5 Point absorber hypothesis

5.1 Evidence for increased scattering

To verify the hypothesis of small angle scattering increase in the arm cavities, the power on the *payload baffle targets* has been monitored (figure 18). Four targets are installed on each of the outer payload baffles with the aim of easing the pre-alignment procedure of the leaser beam to the arm cavities. The targets, 20mm×30mm in size, have rough surfaces to enhance the scattering efficiency so to be easily visible with the camera installed at one of the tower viewports.
During the dark fringe transition, the integrated power on the targets has been observed to increase and, more precisely, to be anti-correlated with cavity power, as shown in figure 19.
The same signals have been observed during the experiment of the impact point variation on the End test masses surface described in section 4.1, as reported in figure 20: also in this case, the power trend on the targets results to be anti-correlated with the intra-cavity power.
This test suggests once again the hypothesis of a point absorber on one or both the test masses.

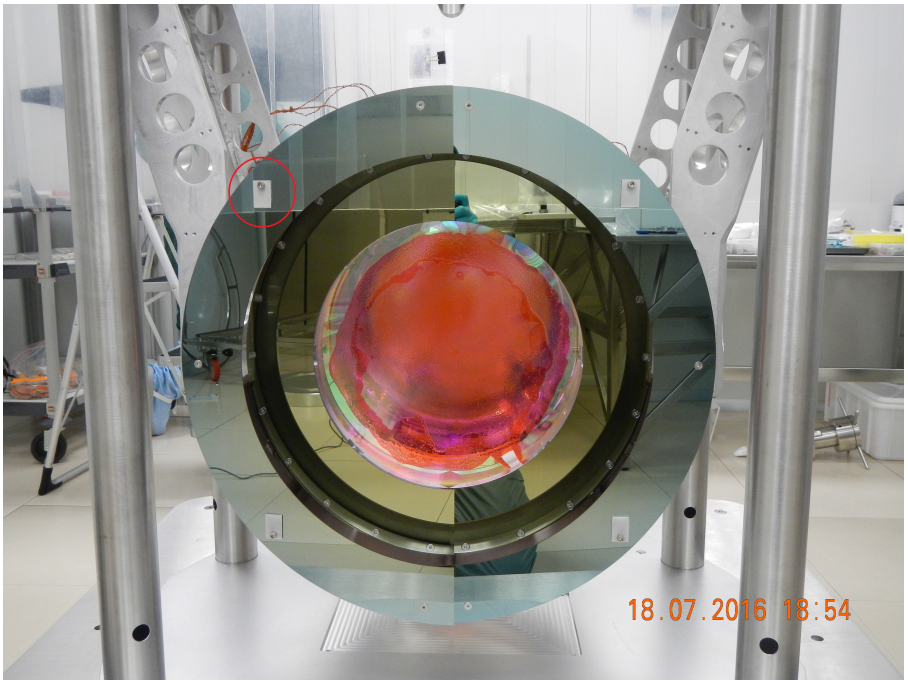

Figure 18: Payload baffles around one of the test masses. Four aluminum targets (as the one highlighted by the red circle) are installed on the external baffle with the aim of easing the beam pre-alignment procedure. During the dark fringe transition, the total power on these targets is used to monitor the light scattered from the mirror in the arm cavity. See text for further details.

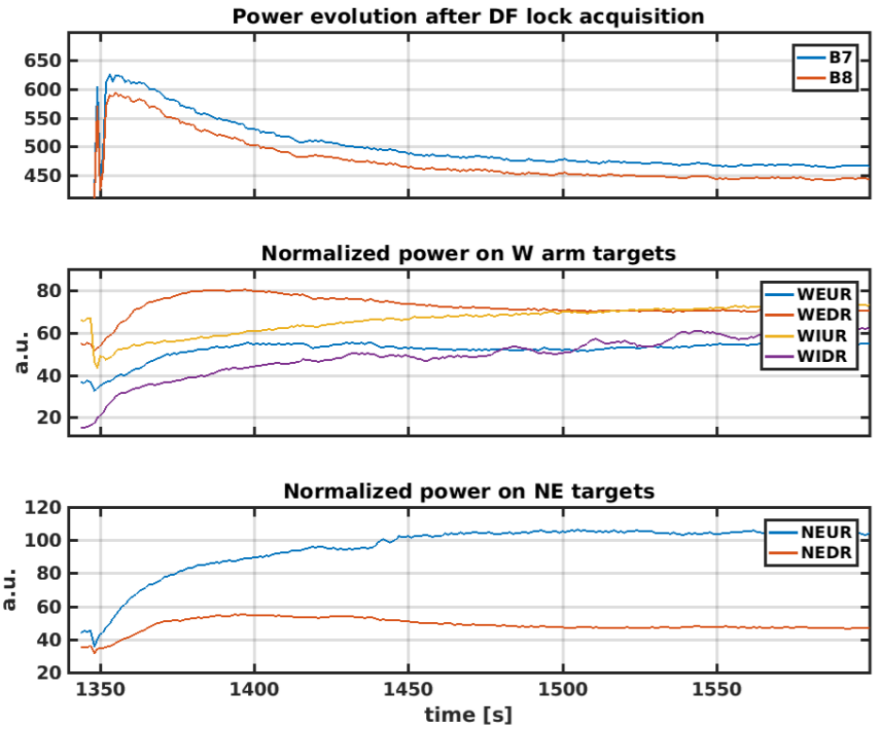

Figure 19: Power on the baffles during the dark fringe transition. Top plot: power trend in the arms. Mid plot: normalized power on the four targets on the West End payload. Bottom plot: Normalized power on two out of the four targets on the North End payload, the other two being out of the camera field of view. The normalized illumination on the payload targets anti-correlate with the cavity power.

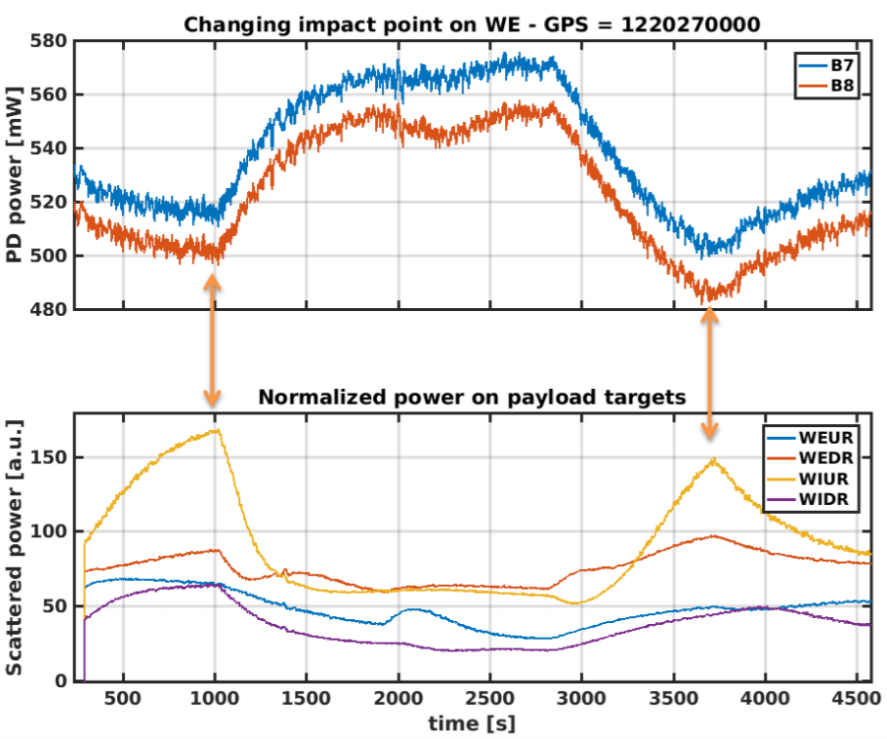

Figure 20: Power on the baffles during the dark fringe transition. Top plot: power trend in the arms. Bottom plot: normalized power on the four targets on the West End payload, the other two being out of the camera field of view. The normalized illumination on the payload targets anti-correlate with the cavity power.

5.2 Simulations on point absorber

To shore up the point absorber hypothesis, an FFT simulation has been performed using SIS [9]. The power recycled interferometer configuration has been considered, and the power absorbed by the point defect has been set to 30 mW. As for the experiment, the beam position has been displaced on one of the ETMs, following the 11 position shown in the subfigure (which is a thumbnail of fig. 14) and the intracavity power variation has been computed for each position. The result is shown in the top plot of figure 21, which reproduces pretty well the experimental behavior shown in figure 20. Furthermore, in the bottom plot the normalized power scattered at the same distance as the targets on the baffles has been reproduced. In this case, the analogy with the data is not straightforward, since also the camera orientation angle and possible image flip could influence the percentage of power in the upper or lower target. However, also in this case the correspondence between simulations results and measurements seem to be pretty good.
These simulations show that the performed measurements are compatible with the hypothesis of a point defect absorbing 30mW put at (10mm, -11mm) from the mirror center.

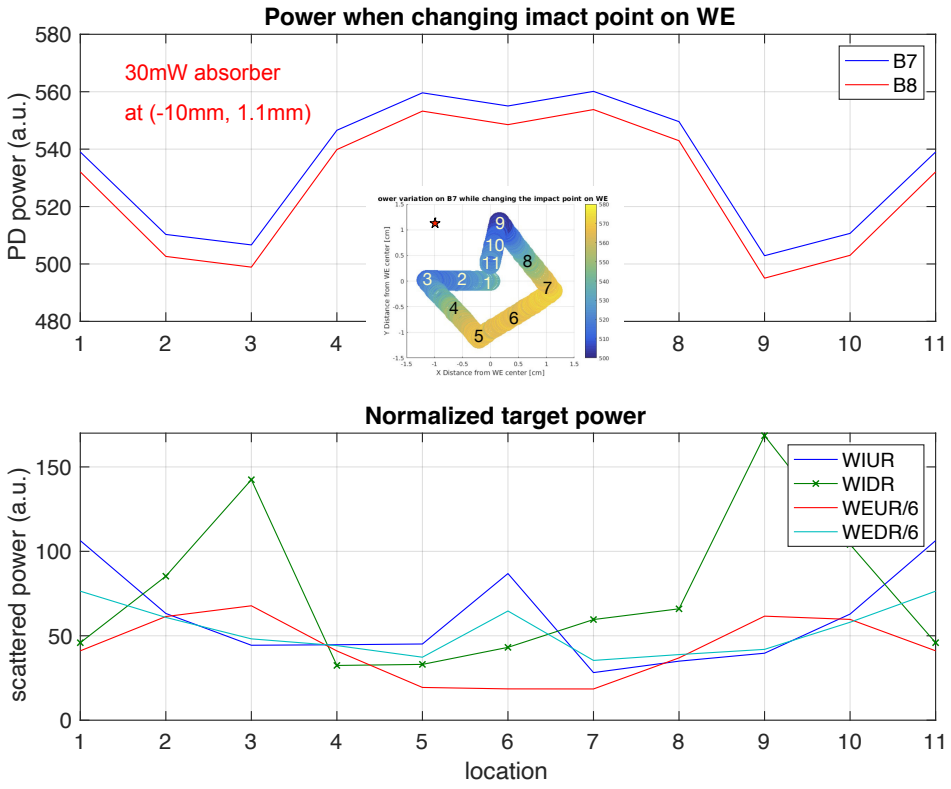

Figure 21: Top: Simulation of arm cavity power in presence of a point absorber at (10mm, -11mm) from the mirror center - represented with a red star - while moving the beam position on the West End Test Mass. This simulation reproduces quite well the experimental results reported in top plot of figure 20. Bottom plot: simulated scattered power on the targets. Also in this case, the resulting power trend is in a good agreement with the measurements shown in 20, bottom plot.

6 Conclusions

Since the beginning of the dark fringe lock in Advanced Virgo, a power drop of about 10% in the Fabry-Perot cavities has been observed. Many investigations were performed to understand the nature of this drop, and few hypotheses were discarded.
Simulations showed that defects regarding the coupling of the laser beam to the interferometer, like mismatch, misalignment or longitudinal offsets do not give rise to a trend of power compatible with what has been observed. Also a fake drop due to the heating of electronics has been ruled out, as the effect is seen by all the photodetectors, quadrant photodiodes, and cameras. This effect is experienced only by the carrier field, as the sidebands don't seem to be affected by the same trend, suggesting that the process is probably taking place in the arms rather than in the central interferometer. Finally, it is not explained as losses towards the dark fringe. The only hypothesis which seems to give rise to this phenomenon is a variation of losses in both the arms.
The drop percentage and the time constant of the process have been studied for different input power. The outcome is that the drop percentage increases with the input power, while the time constant seems to undergo a very little change, if any, not proportional to the power drop percentage increase. Finally, an experiment was performed to better understand the nature of the drop: the beam spot position has been changed on the End test masses surfaces, and a working condition was found where all the circulating power was recovered. After this test, the possible mechanism was identified as related to the presence of a point absorber on the mirror surface: at the dark fringe transition, the circulating power in the arms is absorbed by the point imperfection, which blows up and scatters light towards high order modes whose resonance condition is fulfilled close to the TEM00 resonance. Because of their high mode order (8 or 9), their spatial distribution is wider than the TEM00 ($\sqrt{8}$ or $\sqrt{9}$ times larger), and some of their light is scattered off the cavity axis. This should be the mechanism driving the power drop. To move these modes away from the resonance, the radii of curvature of the end test masses was changed, until part of the circulating power was recovered, as the resonance condition for some of the HOMs was no longer fulfilled.
In order to further prove this hypothesis, an FFT simulation was performed, and it was found that a point defect absorbing 30mW situated at about 1 cm from the mirror center can reproduce the observed power drop percentage and RTL increase.
Despite of this analysis, this is not a conclusive picture, although there are many hints pointing towards some spurious thermal effects driven by at least one point defect, whose origin is still unclear (impurity in the coating, dust particle, ...).
This effect has to be properly taken into account mostly in view of increasing the circulating power, as it would lower the efficiency of optical gain (and therefore sensitivity) increase.

References

[1] A. Chiummo, A. Allocca, P. Ruggi and the Commissioning crew - Power drop recap - VIR-0625A-18 (Virgo presentation). 1

[2] A. Allocca and A. Chiummo for the OptChar team - Optical characterization update - VIR-0667A-18 (Virgo presentation). 1

[3] P.Ruggi, personal communications. 2

[4] The Virgo collaboration, "Advanced Virgo TDR", pag 331, VIR-0128A-12. 1

[5] R. A. Day *et al.* Reduction of higher order mode generation in large scale gravitational wave interferometers by central heating residual aberration correction - *Phys. Rev. D* **87** 082003 - 2013. 10

[6] A. Allocca - Proposal for scattered light investigation - VIR-0423A-18 (Virgo presentation). 10

[7] I. Nardecchia for the TCS and commissioning teams - tests with ETM RHs - VIR-0624A-18 (Virgo presentation). 10

[8] I. Nardecchia, L. Aiello, E. Cesarini, V. Fafone, M. Lorenzini, Y. Minenkov , A. Rocchi, V. Sequino - Status of the art of the Advanced Virgo TCS. G1900595 (LIGO - Virgo presentation). 10

[9] Y. Yamamoto - SIS (Stationary Interferometer Simulation) manual. LIGO-T070039-v8. 17